



Semnan University



Time Dependent Heat Source Estimation by Conjugate Gradient Method in Multi-Layers System for Hyperthermia of Breast cancer

Mansoureh Shariatmadar tehrani^a, Mohammad Mohsen Shahmardan^a,
 Mohammad Hasan Kayhani^a, Mohammad Mohammadiun^{*,b}

^a Mechanical Engineering Dep., Shahrood University of Technology, Shahrood, Iran.

^b Department of mechanical engineering, Shahrood branch, Islamic azad university, Shahrood, Iran.

PAPER INFO

Paper history:

Received: 2020-02-02

Revised: 2020-05-10

Accepted: 2020-05-19

Keywords:

Hyperthermia;
 Heat source;
 Pennes bioheat equation;
 General coordinate method;
 Inverse method.

ABSTRACT

Hyperthermia is a form of cancer treatment where the temperature of the tumor is elevated to levels that induce its elimination. This paper discusses using a heating power source to destroy breast cancer cells. The geometry of the breast tissue is represented as a hemisphere containing three layers; muscle, gland, and fat. The conjugate gradient method was used to solve the inverse heat conduction problem via the Pennes bioheat equation in an axisymmetric coordinate system, where the irregular region in the physical domain (r,z) was transformed into a rectangle in the computational domain (ξ, η) . The performance of the algorithm was evaluated on a tested point located at the $(5, 2)$ position, accounting for two temperature increments. The results confirmed the accuracy and viability of the algorithm, which makes this approach promising for the actual application for breast cancer treatment soon.

DOI: 10.22075/jhmtr.2020.19707.1277

© 2020 Published by Semnan University Press. All rights reserved.

1. Introduction

The notoriety of cancer makes it a popular research topic across the world, especially research on cancer treatments. Cancer treatment encompasses surgery, chemotherapy, radiation therapy. As cancer cannot be easily treated via conventional therapies, there is interest in developing new methods that could enhance the effects of conventional cancer treatment approaches. A practical method that can be used in conjunction with conventional therapies is the hyperthermia approach, where the temperature of tumor-loaded tissue is raised to 40-43°C for a preset period while leaving the healthy regions unheated. Exposure to higher temperatures renders the cancer cells more susceptible to radiation (radiotherapy) or chemicals (chemotherapy) [1]. Despite its promising premise, hyperthermia suffers from one glaring drawback: targeted temperature control, where the tumors are targeted and heated while the healthy cells are left intact. Hyperthermia has been reported to be useful for eliminating head and neck tumors, and chest, brain,

bladder, cervix, rectum, lung, vagina, and skin cancers. A mathematical model of heat transfer in a 3-layer tissue in a limited space was constructed to estimate the temperature control profiles in hyperthermia conditions. Hyperthermia is heavily dependent on the features of its respective heat sources. Also, due to the position of the tumors, hyperthermia can be utilized in three different ways; local hyperthermia, regional hyperthermia, and whole-body hyperthermia (WBH) vis-à-vis therapeutic applications for treating cancer [2]. Heat transfer with in multi-layer tissue is a complicated procedure [3] due to its inclusion of multiple mechanisms such as conduction in tissue, convective tissue in the blood, and diffusion of blood and its dissemination in micro-granular cells. The complexity of heat transfer with in living tissue makes it challenging to construct an accurate and representative mechanical model envisioning the entire process. Hypotheses and simplifications alongside essential features of the process need to be accounted for when constructing mechanical models to represent the above

*Corresponding Author: Mohammad Mohammadiun, Mechanical Engineering Dep., Islamic Azad University, Shahrood Branch, Shahrood, Iran.

Email: mmohammdiun@yahoo.com

mentioned cases. There are two types of heat conduction solution, which are direct and inverse methods [1, 4].

Generally, there are three different models of heat transfer biomass equations: Pennes bioheat transfer model [5], thermal wave bioheat transfer model [6, 7], and dual-phase-lag heat transfer model [8]. The Pennes bioheat equation was published in 1948 [5] and was deemed suitable due to its simplicity and applicability in specific conditions. The Pennes bioheat equation relies on critical factors such as equilibration site, blood perfusion, vascular architecture, and blood temperature [5]. Pennes was the first researcher to study tissue and blood temperature in the resting human forearm. Moreover Pennes was succeed to estimate an appropriate modification to the standard heat equation through introducing a blood perfusion term. Lu et al. [9] investigated to find a basic solution for thermal wave model of bioheat transfer and achieved this solution is complicated. Many researches has been done in different analytical and numerical methods to find the solution for the bioheat transfer problems [10]. Most of researches was done numerically. Ahmadikia et al. [11] used Laplac transform method and solve the Pennese bioheat equation while assuming the heat flux boundary conditions are constant, periodic and pulse train for skin as a semi-infinite and finite domain. Shih et al. [12] also applied Laplace transform method to solve the Pennes bioheat equation and analyzed the effect of the temperature response of the semi-infinite biological tissue. Same as these type of methods, Yuan [13] studied on biological tissue immersed in water with a sinusoidal temperature alternation on the skin surface to simulate the contrast therapy by accounting the transient temperature response. Tung et al.[14] suggested an improved 1-D Hyperbolic heat transfer equation (HHTE) and recommended significant changes to parabolic and hyperbolic models. Cotta et al. [15] suggested a 'generalized integral transform technique' (GITT) for solving the 1-D PBHE equation based on assumptions such as constant and lined thermo-physical characteristics and the amount of blood perfusion. Lee et al. [16] estimated the surface heat flux using an inverse hyperbolic heat conduction method in living tissue. They proposed an inverse algorithm based on the conjugate gradient method. The difference approach for solving the hyperbolic heat transfer problem was utilized to estimate the time-independent surface heat flux in a living tissue from the temperature measurement within the tissue. Mohammadiun et al. used the conjugate gradient method to estimate the time-dependent heat flux in multi-layers systems by solving the inverse method [17-19]. Jalali et al.[20] studied factors that affect living tissues via heat treatment. The premise of his work is the fact that temperature distribution and control are crucial vis-à-vis hyperthermia. Emanuei et al. [21] constructed a simplified 1-D model of heat transfer of spherical biological living tissue based on the Pennes bioheat equation by taking into account the constant blood perfusion prevalent in heat transfer problems, while Baghban et al. [22] proposed a sequential technique to determine the heating power of an

external source. Dutta and Kondu [2] proposed an exact analytical solution of a thermal profile of a 1-D Pennes' bioheat equation (PBHE) in living tissue via the separation of variables method, and the solution is expected to influence thermal treatments. Dutta and Kondu [3] also proposed a 2-D Pennes' bioheat equation (PBHE) to describe heat treatments using Fourier and non-Fourier heat transfer methods.

In presented research, the conjugate gradient method, coupled with an adjoint equation approach is employed, to solve the inverse heat conduction problem and to predict the power of the heat source using temperature distribution at two central points in a multi-layers system. The equations are solved using the finite difference method in an axisymmetric coordinate system. It is the first time where an axisymmetric model is employed to solve the Pennes equation within a multilayer system and is the most important innovation of the paper. The irregular region in the physical domain (r, z) is transformed into a rectangle in the computational domain (ξ, η) . The present formulation is general and can be applied to the solution of boundary inverse heat conduction problems over any region that can be mapped into a rectangle. The governing equations are solved by employing the finite difference method. The obtained results show that the applied method causes high stability, even if the input data includes considerable noise.

The next section details the problem formulation and geometry design, and Section 2. explained mathematical method of solution, then section four discusses the results, and section five concludes this paper.

2. Problem formulation and Geometry Design

The axisymmetric cylindrical coordinate system (r, ϕ, z) was used to solve the problem on the z -axis. Therefore, the derivative of the variables with respect to ϕ is zero. Fig 1.a shows a 3D model of the breast, while Fig1.b shows the boundary conditions and different layers of the problem. The geometry of the breast was assumed to be a hemisphere, as shown in Fig.1.a.

The energy equation was set into a cylindrical coordinate system (r, z) , then transformed into a physical coordinate system $(r; z)$; the results are shown in Fig 2. By rotating the model around the z -axis, a semispherical model was obtained. As shown in Fig. 2, the time-dependent heating power source is employed on the exterior surface, while the heat source is located in the tissue.

It is necessary to predict the unknown heating power source $G_p(t)$ on the external surface during $0 \leq t \leq t_f$, where t_f is the final time, using the temperature distribution at a specific point. It should also be pointed out that noise affects the input data in this case. The numerical solution was obtained using the general coordinate method.

The results garnered from solving the problem in the rectangular coordinate system (ξ, η) was transformed to

Table 1. Physical properties of breast tissue

	h (mm)	k (W/mK)	ρ (kg/m ³)	C(J/kgK)	q'''_m (W/m ³)
Fat	5.0[25]	0.21[23]	930[24]	2770[24]	400[23]
Gland	43.4[25]	0.48[23]	1050[24]	3770[24]	700[23]
Muscle	15[25]	0.48[23]	1100[24]	3800[26]	700[23]
Tumor	--	0.48[23]	1050[24]	3852[26]	5000[27]

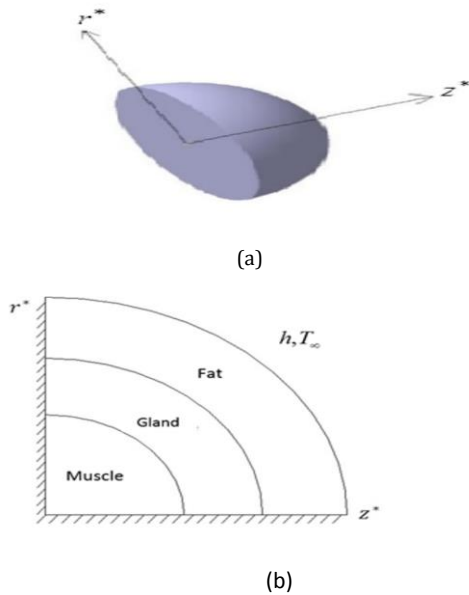


Figure 1. a) Geometry of breast b) boundary conditions of the problem

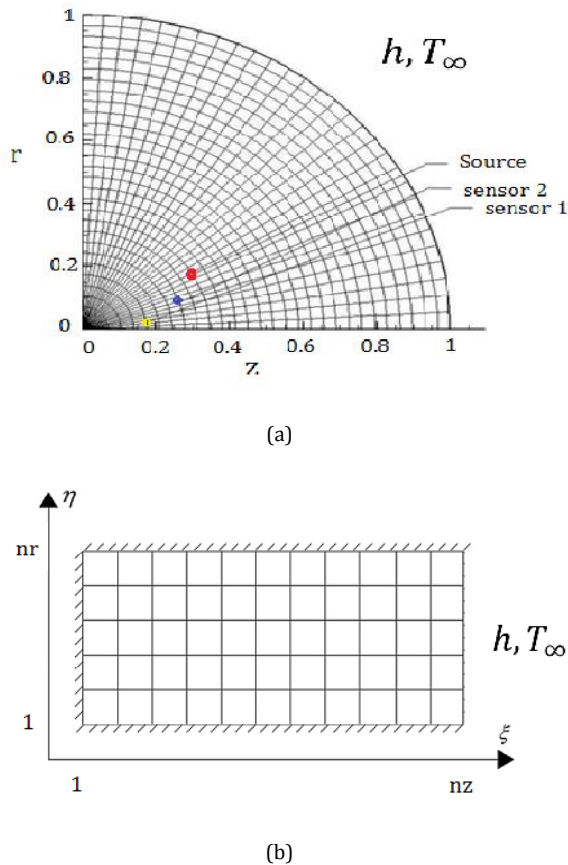


Figure 2. a) Physical and b) computational domains

the physical coordinate system (r,z), with the computational plane shown in Fig 2.b, and its related boundary conditions presented in Fig. 3.

3. Mathematical Method

In this work, the definition of heat transfer in soft tissue is based on the Pennes bioheat equation [5], where it was assumed that the total energy exchange of the flowing blood is related to the volumetric heat flow and the blood and tissue temperature gradient.

3.1. Direct problem

The equation for describing the 3-D expression of the Pennes bioheat in a living tissue when the physical properties remains unchanged is:

$$\nabla^2(KT) + \rho_b C_b \dot{W}_b (T_{a0} - T) + q'''_m + G_p(t) \delta(r - r^{**}) \delta(z - z^{**}) = \rho c \frac{\partial T}{\partial t} \quad (1)$$

Where T is the temperature, K is the tissue thermal conductivity, ρ_b is the blood density, C_b is the blood specific heat, \dot{W}_b is the blood perfusion rate, T_{a0} is the arterial temperature, q'''_m is the metabolic heat generation rate, δ is the Dirac delta function, t is the time, ρ is the tissue density, and c is the tissue-specific heat. The real values that can describe the physical properties of the breast tissue are tabulated in Table 1 [23-27].

In the cylindrical coordinate system, the Pennes bioheat equation, considering the axisymmetric condition, is:

$$\frac{1}{r} \frac{\partial}{\partial r} \left(Kr \frac{\partial T}{\partial r} \right) + \frac{\partial}{\partial z} \left(K \frac{\partial T}{\partial z} \right) + \rho_b C_b \dot{W}_b (T_{a0} - T) + q'''_m + G_p(t) \delta(r - r^{**}) \delta(z - z^{**}) = \rho C \frac{\partial T}{\partial t} \quad (2)$$

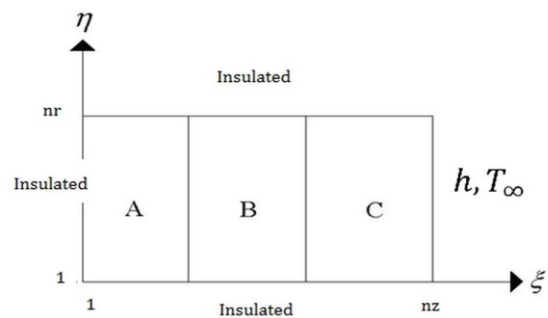


Figure 3. Boundary condition in a computational plane

K is not dependent on temperature and is different in the case of each tissue.

It is assumed that the variables are dimensionless, and K is constant for every type of tissue:

$$r^* = \frac{r}{R}, \theta = \frac{T - T_{a0}}{qR/K}, t^* = \frac{\alpha t}{R^2}, Z^* = \frac{z}{R} \quad (3)$$

Where θ is the elevation temperature.

The following equation, derived in the dimensionless form is:

$$\frac{\partial^2 \theta}{\partial r^{*2}} + \frac{1}{r^*} \frac{\partial \theta}{\partial r^*} + \frac{\partial^2 \theta}{\partial z^{*2}} - \frac{\rho_b C_b \dot{W}_b R^2}{K} \theta + \frac{q'' R}{q_0} + G_p(t^*) \delta(r^* - r^{**}) \delta(z^* - z^{**}) = \frac{\partial \theta}{\partial t^*} \quad (4)$$

The boundary conditions are detailed below:

On the left and down boundaries:

$$\frac{\partial \theta}{\partial n} = 0 \quad (5)$$

On the outer boundary:

$$q - q_c = 0 \rightarrow q = q_c \quad (6)$$

On the other hand:

$$-k \frac{\partial T}{\partial n} = h(T - T_{\infty}) \quad (7)$$

$$T = \frac{q_0 R}{K} \theta + T_{a0} \rightarrow \frac{\partial T}{\partial n} = \frac{q_0 R}{K} \frac{\partial \theta}{\partial n} + 0$$

$$-K \frac{\partial T}{\partial n} = -q_0 R \frac{\partial \theta}{\partial n} \quad (8)$$

$$\theta_{\infty} = \frac{T_{\infty} - T_{a0}}{\frac{q_0 R}{K}} \rightarrow T_{\infty} = \frac{q_0 R}{K} \theta_{\infty} + T_{a0}$$

$$T - T_{\infty} = \frac{q_0 R}{K} (\theta - \theta_{\infty}) \quad (9)$$

Combining equations (7), (8), and (9), we obtain:

$$-q_0 R \frac{\partial \theta}{\partial n} = h \frac{q_0 R}{K} (\theta - \theta_{\infty}) \quad (10)$$

Furthermore, by applying the boundary conditions on to the top boundary, we obtain:

$$\frac{\partial \theta}{\partial n} = -\frac{h}{K} (\theta - \theta_{\infty}) \quad (11)$$

$$\theta(z^*, r^*, 0) = 0 \quad (12)$$

Where the unit for h is $\frac{W}{m^2 K}$, while the unit for K is $\frac{W}{mK}$.

The transformation of the physical domain to the computational domain are discussed in details in the Appendix.

The boundary conditions in the computational domain are:

$$\xi = 1 \rightarrow \frac{1}{J\alpha^{\frac{1}{2}}} (\alpha\theta_{\xi} - \beta\theta_{\eta}) = 0 \quad (13)$$

$$\xi = nz \rightarrow \frac{1}{J\alpha^{\frac{1}{2}}} (\alpha\theta_{\xi} - \beta\theta_{\eta}) = -\frac{h}{k} (\theta - \theta_{\infty}) \quad (14)$$

$$\eta = 1, \eta = nr \rightarrow \frac{1}{J\gamma^{\frac{1}{2}}} (-\beta\theta_{\xi} - \gamma\theta_{\eta}) = 0 \quad (15)$$

In the interface of tissues shown in Fig. 3, the following relations are used, while Fig 3. a, b, and c represent the muscle, glands, and fat tissues, respectively.

$$q_{\xi in} + q_{\eta in} = q_{\xi out} + q_{\eta out} \quad (16)$$

$$k_A(\theta_{i,j} - \theta_{i-1,j}) + \frac{2k_A k_B}{k_A + k_B} (\theta_{i,j} + \theta_{i-1,j}) = k_B(\theta_{i+1,j} - \theta_{i,j}) + \frac{2k_A k_B}{k_A + k_B} (\theta_{i,j+1} + \theta_{i,j}) \quad (17)$$

$$k_B(\theta_{i,j} - \theta_{i-1,j}) + \frac{2k_C k_B}{k_C + k_B} (\theta_{i,j} + \theta_{i-1,j}) = k_C(\theta_{i+1,j} - \theta_{i,j}) + \frac{2k_C k_B}{k_C + k_B} (\theta_{i,j+1} + \theta_{i,j}) \quad (18)$$

3.2. Inverse problem

The time-dependent heating power source in the inverse problem can be solved by accounting for the measured transient temperatures, estimated in the location of two sensors at two specific points. The following function must be minimized to solve the inverse problem [28]:

$$S[G_p(t^*)] = \frac{1}{2} \int_{t^*=0}^{t^*=t_f^*} \sum_{m=1}^{N_s} [\theta(\xi_m, \eta_m, t^*, G_p) - Y_m(t^*)]^2 dt^* \quad (19)$$

Where $\theta(\xi_m, \eta_m, t^*, G_p)$ is the predicted temperature and $Y_m(t^*)$ is the measured temperature. The number of sensors, N_s , is 2.

3.3. Adjoint problem

The conjugate gradient method can be used to minimize equation (19). Determining the direction of an unidentified heating power source in the conjugate algorithm depends on the gradient of the error function and the solution by the adjoint equations [28-30], best described by the equation below:

$$\frac{\partial^2 \lambda}{\partial r^{*2}} + \frac{1}{r^*} \frac{\partial \lambda}{\partial r^*} + \frac{\partial^2 \lambda}{\partial z^{*2}} - \frac{\rho_b C_b \dot{W}_b R^2}{K} \lambda + \sum_{m=1}^{N_s} [\theta(\xi, \eta, t^*, G_p) - Y_m(t)] \delta(\eta - \eta_m) \delta(\xi - \xi_m) = \frac{\partial \lambda}{\partial t^*} \quad (20)$$

In the interface of the materials, using the model shown in Fig. 3, the reactions below are used:

$$k_A(\lambda_{i,j} - \lambda_{i-1,j}) + \frac{2k_A k_B}{k_A + k_B} (\lambda_{i,j} + \lambda_{i-1,j}) = k_B(\lambda_{i+1,j} - \lambda_{i,j}) + \frac{2k_A k_B}{k_A + k_B} (\lambda_{i,j+1} + \lambda_{i,j}) \quad (21)$$

$$\begin{aligned}
 k_B(\lambda_{i,j} - \lambda_{i-1,j}) + \frac{2k_C k_B}{k_C + k_B}(\lambda_{i,j} + \lambda_{i-1,j}) \\
 = k_C(\lambda_{i+1,j} - \lambda_{i,j}) \\
 + \frac{2k_C k_B}{k_C + k_B}(\lambda_{i,j+1} + \lambda_{i,j})
 \end{aligned}
 \tag{22}$$

The boundary conditions are as follows:

$$\frac{\partial \lambda}{\partial n} = 0
 \tag{23}$$

$$\lambda(z^*, \gamma^*, t_f^*) = 0
 \tag{24}$$

Where n is the normal vector at the surface.

The boundary conditions in the computational plane, shown in Fig. 3 are as follows:

$$\xi = 1, \xi = n_z \rightarrow \frac{1}{J\alpha^2}(\alpha\lambda_\xi - \beta\lambda_\eta) = 0
 \tag{25}$$

$$\eta = 1, \eta = n_z \rightarrow \frac{1}{J\alpha^2}(-\beta\lambda_\xi - \gamma\lambda_\eta) = 0
 \tag{26}$$

3.4. Sensitivity problem

The perturbing $G_p(t^*)$ is changed by $\Delta G_p(t^*)$, and in the same manner by $\theta(r^*, z^*, t^*)$ and $\Delta\theta(r^*, z^*, t^*)$ to obtain the sensitivity equation. Therefore, in direct solving method the variables $\theta(r^*, z^*, t^*)$ and $G_p(t^*)$ are replaced by $[\theta(r^*, z^*, t^*) + \Delta\theta(r^*, z^*, t^*)]$ and $[G_p(t^*) + \Delta G_p(t^*)]$ respectively, and its final expression can be subtracted from the direct problem [28], resulting in:

$$\begin{aligned}
 \frac{\partial^2 \Delta\theta}{\partial r^{*2}} + \frac{1}{r^*} \frac{\partial \Delta\theta}{\partial r^*} + \frac{\partial^2 \Delta\theta}{\partial z^{*2}} - \frac{\rho_b C_b W_b R^2}{K} \Delta\theta \\
 + \frac{q''' R}{q_0} \\
 + \Delta G_p(t) \delta(r^* - r^{**}) \delta(z^* - z^{**}) = \frac{\partial \Delta\theta}{\partial t^*}
 \end{aligned}
 \tag{27}$$

Where $\Delta\theta$ is the sensitivity temperature. In the interface of the materials, using the model shown in Fig. 3, the equations below were used:

$$\begin{aligned}
 k_A(\Delta\theta_{i,j} - \Delta\theta_{i-1,j}) \\
 + \frac{2k_A k_B}{k_A + k_B}(\Delta\theta_{i,j} + \Delta\theta_{i-1,j}) \\
 = k_B(\Delta\theta_{i+1,j} - \Delta\theta_{i,j})
 \end{aligned}
 \tag{28}$$

$$\begin{aligned}
 k_B(\Delta\theta_{i,j} - \Delta\theta_{i-1,j}) \\
 + \frac{2k_C k_B}{k_C + k_B}(\Delta\theta_{i,j} + \Delta\theta_{i-1,j}) \\
 = k_C(\Delta\theta_{i+1,j} - \Delta\theta_{i,j}) \\
 + \frac{2k_C k_B}{k_C + k_B}(\Delta\theta_{i,j+1} + \Delta\theta_{i,j})
 \end{aligned}
 \tag{29}$$

boundary conditions on the left and down boundaries are:

$$\frac{\partial \Delta\theta}{\partial n} = 0
 \tag{30}$$

on the top boundary:

$$\frac{\partial \Delta\theta}{\partial n} = -\frac{h}{K} \Delta\theta
 \tag{31}$$

The boundary condition in the computational plane are:

$$\xi = 1 \rightarrow \frac{1}{J\alpha^2}(\alpha\Delta\theta_\xi - \beta\Delta\theta_\eta) = 0
 \tag{32}$$

$$\xi = n_z \rightarrow \frac{1}{J\alpha^2}(\alpha\Delta\theta_\xi - \beta\Delta\theta_\eta) = -\frac{h}{K} \Delta\theta
 \tag{33}$$

$$\eta = 1, \eta = n_r \rightarrow \frac{1}{J\gamma^2}(-\beta\Delta\theta_\xi - \gamma\Delta\theta_\eta) = 0
 \tag{34}$$

The gradient equation is:

$$\nabla S[G_p(t^*)] = \lambda(\xi, \eta, t^*)
 \tag{35}$$

There is a dependency between the above equality and the position of the unknown function.

3.5. Iterative method

The estimation of the heat source power $G_p(t^*)$ as an unknown function is realized via function minimization.

The repetitive function for estimating $G_p(t^*)$ is [28, 29, 31]

$$G_p^{k+1}(t^*) = G_p^k(t^*) - \beta^k d^k(t^*)
 \tag{36}$$

Moreover, k is assumed to be the iteration number.

The estimation of $d^k(t^*)$ as the direction of descent is estimated to be [28, 30, 31]:

$$d^k(t^*) = \nabla S[G_p^k(t^*)] + \gamma^k d^{k-1}(t^*)
 \tag{37}$$

Where γ^k is the conjugate coefficient [28, 29, 32], and can be acquired by:

$$\gamma^k = \frac{\int_{t^*=0}^{t_f^*} \{\nabla S[G_p^k(t^*)]\}^2 dt^*}{\int_{t^*=0}^{t_f^*} \{\nabla S[G_p^{k-1}(t^*)]\}^2 dt^*}
 \tag{38}$$

$$\beta^k = \frac{\int_{t^*=0}^{t_f^*} \sum_{m=1}^{N_s} [\theta(\xi_m, \eta_m, t^*, G_p^k) - Y_m(t^*)] \Delta\theta(\xi_m, \eta_m, t^*, d^*) dt^*}{\int_{t^*=0}^{t_f^*} \sum_{m=1}^{N_s} [\Delta\theta(\xi_m, \eta_m, t^*, d^*)]^2 dt^*}
 \tag{39}$$

Where γ^0 is assumed to be zero.

The searching rate, β^k , can be determined by minimizing $S[G_p^{k+1}(t^*)]$ and considering β^k to be: (39)

In the above equation, the assumption of $\Delta G_p^k(t^*) = d^k(t^*)$ help realizes $\Delta\theta(\xi_m, \eta_m, t^*, d^*)$ the sensitivity problem.

Whenever the stop condition occurs, the mentioned iterative procedure will end. The definition of stopping criterion is:

$$S[G_p(t^*)] \leq \varepsilon
 \tag{40}$$

In the equation (40), $S[G_p(t^*)]$ is obtained using equation (19). The value of ε should be chosen, and while errors exist in the measured data, the results would be accurate.

3.6. Computational algorithm

The computational process to determine the hidden heating power source is summarized as follows [28]:

1. Select a primary presumption, for instance $G_p^0(t^*)$, in the function $G_p(t^*)$, by setting k as zero.
2. Calculate $\theta(z^*, r^*, 0)$ by solving the direct problem based on $G_p^k(t^*)$ (Eqs. (1-15, A1-A16)).

3. Continue if the stop condition does not occur, or else stop (Eq. (40)).
4. Find the solution of the adjoint problem, and calculate $\lambda(z^*, r^*, t^*)$ by knowing $\theta(\xi_m, \eta_m, t^*, G_p)$ and the term $Y_m(t^*)$ (Eqs. (20-26)).
5. Calculate $\nabla S[G_p^k(t^*)]$ in Eq. (35) by using achieved $\lambda(\xi_m, \eta_m, t^*)$ from the previous step.
6. Calculate γ^k and $d^k(t^*)$ from Eq. (38) and Eq. (37), respectively, using achieved $\nabla S[G_p^k(t^*)]$ from the previous step.
7. Calculate $\Delta\theta(\xi_m, \eta_m, t^*, d^*)$ in the sensitivity problem by setting $\Delta G_p^k(t^*) = d^k(t^*)$ Eq. (39)).

Table 2. The RMS errors between the exact and estimated values for the different functions

σ	function	RMS Error
0	Linear	0.121
	Sin-Cos	0.273
	step	0.312
0.01T _{max}	Linear	0.553
	Sin-Cos	0.117
	step	0.332

8. Knowing β^k from Eq. (39) based on achieved $\Delta\theta(\xi_m, \eta_m, t^*, d^*)$.
9. Knowing β^k and $d^k(t^*)$, compute $G_p^{k+1}(t^*)$, then back to number 1 (Eq. (36))

4. Results and discussion

This work is predicated on determining the most suitable heat power source that can be used to kill tumors without damaging healthy cells. The heating time was determined to be ~10 minutes. The governing equations were discretized using the finite-difference technique, where a uniform 35×35 dimension mesh size was selected in the numerical method. The prediction of the power source was estimated by measuring the temperature at two points. Fig. 2.a. shows the mesh and locations of the sensors.

4.1. Grid sensitivity

In order to elucidate the independence of the problem from the dimension of the selected mesh, the behavior of presented algorithm is evaluated on three different mesh sizes, such as 35 × 35, 30 × 30 and 25 × 25 and the results are shown in Fig. 4. According to the results, there is no dependency between the size of the mesh and the achieved results. No significant change in the results are observed for three grids of 35 × 35 and 30 × 30 and 25 × 25. Hence the suitable grid for this problem is considered as 35 × 35. The time step was set to be $\Delta t = 0.01$. In order to evaluate the accuracy of the existing solution, three linear functions step, and a combination of sine and cosine functions were employed. It should be pointed out that the discontinuous and sharp corner functions are known to be ill-posed (as

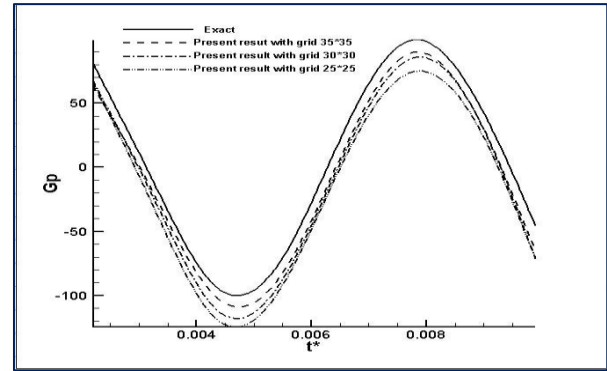


Figure 4. Effect of the mesh size on the final results

shown in Fig. 5.b and Fig. 5.c), and in order to determine the accuracy of the solutions, the functions below (equations 41-43) were selected [28]:

$$h_j = k(c/2)^{-1} \quad (41)$$

$$h_j = k(c/2)^{-1} \quad (42)$$

$$h_j = k(c/2)^{-1} \quad (43)$$

4.2. Sensitivity against noise

The problem sensitivity against noise was evaluated to determine the stability of the presented method. Fig. 5 (a-f) shows a comparison of the estimated heating power source with the exact functions (linear, step, and sin-cosine) with and without noise.

Figs 5. a-c show the comparison of the exact functions of linear, step, and sin-cosine according to the Eq. (41-43) respectively and the related estimated heating power source. It is clear that reaction of the proposed method against step function has a little error comparing other two examined functions however it makes satisfactory. Overall error is negligible and it is mostly related to the high level values or sudden changes. In order to elucidate the actual performance of the proposed solution, another simulation with noisy data was conducted, and the calculation of the noisy data is illustrated by Eq. (44) by applying the noise to data by the amount of $\sigma = 0.01T_{\max}$, where T_{\max} is the maximum temperature, ω is the standard deviation of the normal distribution where $-2.625 < \omega < 2.625$, and σ is the standard deviation of the measured error.

$$h_j = k(c/2)^{-1} \quad (44)$$

Figs 5.d-f shows the influence of noise on the suggested solution performance. Regardless of the noise data, the results look promising. The stability of the algorithm against noise is well, especially for the sin-cosine and step functions, it can be said there is no obvious difference between without noise and with noise results. In the linear function, there is a little difference between mentioned results and adding noise makes some error in the results however it is acceptable yet.

In order to determine the performance of the proposed method, Fig. 6 shows the contours of comparing the estimated heating power source with the exact functions. According to the contours showing in this figure, there are a great match between the estimated heating power source that are shown in Fig 6.a-c and the exact function of temperature distribution showing in Fig 6. d-f. The RMS

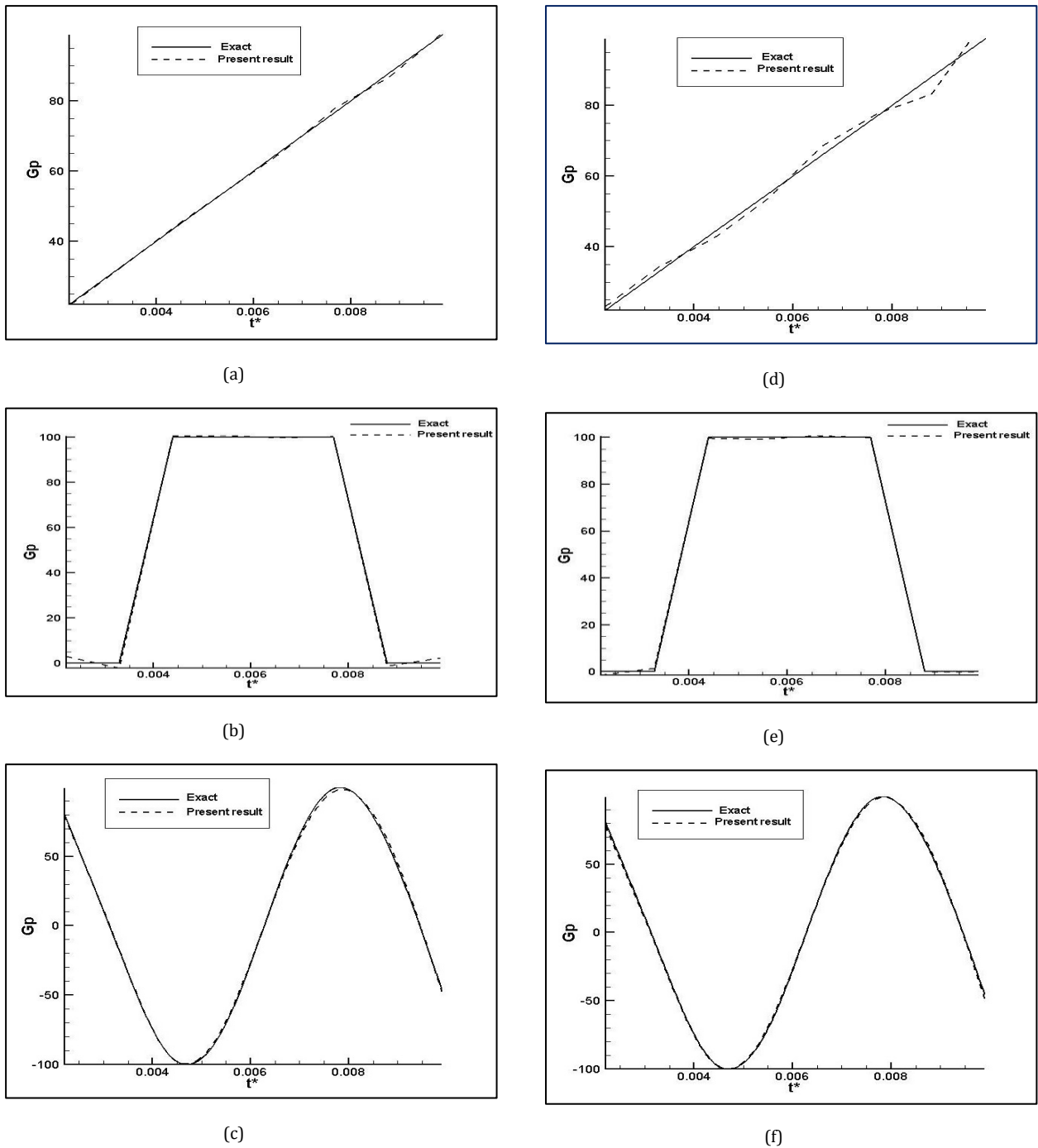


Figure 5. Estimated heating power source compared to the exact function for linear, step, and sin-cosine functions in a three-layer tissue, Figs a-c illustrate the functions without noise, while Figs d-f consist of functions with noise.

errors between the exact and estimated values for the different functions of heating power source are tabulated in Table 2 and estimated by:

Where $G_{ex}(t_i)$ is the heating power source.

$$h_j = k(c/2)^{-1} \tag{45}$$

According to the results in Table 2, it could be assumed that the proposed method behaves well against both data with and without noise. As the step function is known for being highly ill-posed, the related RMS errors are maximum among the examined functions, with the data with the noise and linear function reporting maximum

RMS errors. This means that the noise significantly affects the linear distribution function. The sine-cosine function reported the minimum RMS value.

Considering presented contours in Fig.6, the same results are achieved and for the step function there is more error comparing other two examined functions and sine-cosine function bring better response among all other examined functions. The results indicate same nature of temperature distribution as depicted in case of Fig. 5. But in this case a sharp difference between estimated temperature distribution and estimated temperature

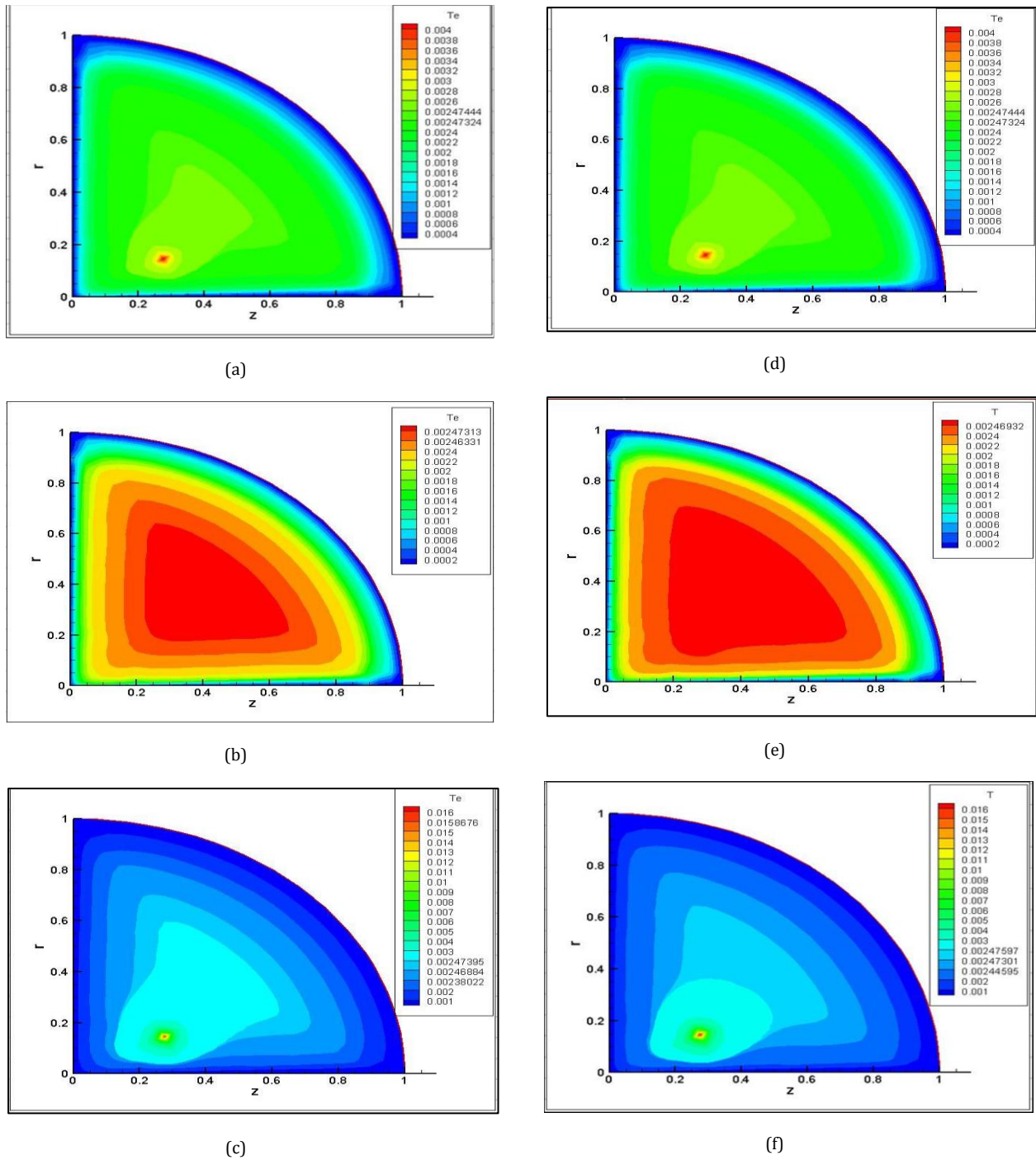


Figure 6. Contours of the exact temperature distribution across a three-layer tissue for linear, step, and sin-cosine functions (a-c), Figures (d-f) illustrates the estimated temperature distribution.

distribution for step function (Figs.6 f, c) has been magnified. In fact there is almost a little variation with respect to all. In other hand the temperature distribution across tissue in all functions in the exact and estimated one are satisfied.

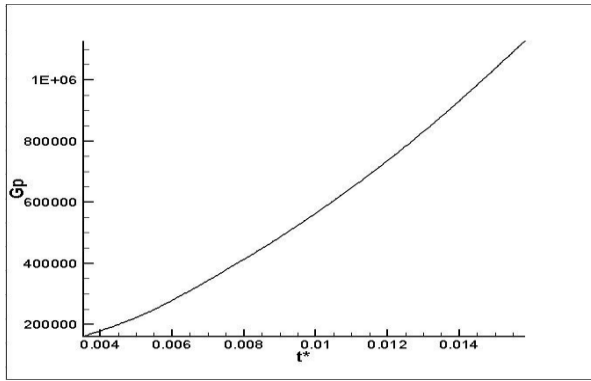
4.3. Time Dependent Heat Source Estimation

The performance of the algorithm was evaluated on a tested point located at position (5, 2) in the physical coordinate system via two different examinations. In the first examination, the temperature was increased

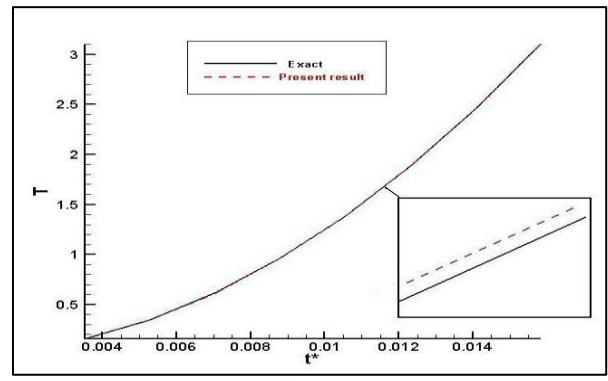
from $T_{a0}=310K$ to $T=318K$ for 10 minutes. The heat equation was transformed into a dimensionless heat equation. It should be pointed out that the dimensionless temperature variable went from $\theta = 0$ to $\theta = 3.84$ in a dimensionless time of $t^*=0.0176$. The dimensionless temperature distribution obeys the parabolic form, as per the following relation:

$$h_j = k(c/2)^{-1} \tag{46}$$

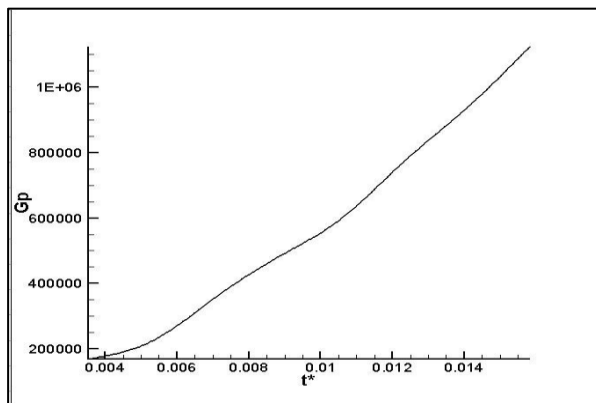
after estimating the coefficient “a,” it was rewritten to:



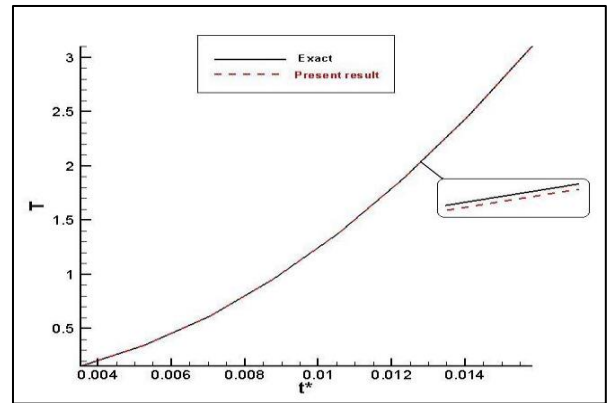
(a)



(a)



(b)



(b)

Figure 7. The estimated heating power source for data without noise (a) and with noise (b)

Figure 8. The comparison of the estimated dimensionless temperature distribution with the exact temperature distribution for data without (a) and with noise (b) for a temperature distribution time of ~10 mins.

$$h_j = k(c/2)^{-1} \tag{47}$$

In order to determine the function of G_p , the problem was solved using the conjugate gradient method and heating power source is achieved, and the results shown in Fig. 7.a, b for both data without and with noise respectively.

To validate the obtained results, G_p is considered as the direct input of the problem and therefore, the temperature distribution at preferred point is found. A comparison between the calculated temperature distribution, and the preferred one, which is the exact one, is illustrated in Fig. 8.

Therefore Fig. 8 shows the results from comparing the estimated dimensionless temperature distribution with the

exact temperature distribution for both data with and without noise for 10 minutes. The results show excellent agreements between the predicted and real values, which means that the algorithm is suitable for use in determining the heating power source. According to the complex presented estimating algorithm, it can follow the changing temperature during the time by pleasing accuracy. The same as the previous examinations, the noise stability examination is applied and the result is shown in Fig. 8.b. and the same accuracy as without noise examination result is achieved. Moreover Fig. 9 shows the related

temperature contours. The temperature contours are good evaluation to determine that the temperature distribution phenomena in biological tissues is satisfied. There is a considerable temperature difference between target point and surrounding regions. Hence, it is a good evidence to prove the presented method is practical.

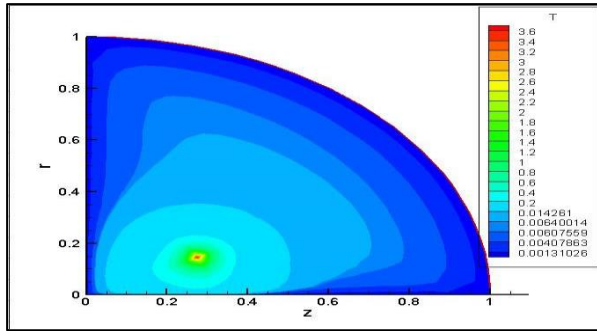
In the next examination, the temperature increment time was assumed to be ~30 minutes. It should be pointed out that the dimensionless temperature variable went from $\theta = 0$ to $\theta = 3.84$ in a dimensionless time of $t^* = 0.0528$. The temperature distribution function is similar to that of the first examination, but the coefficient “a” is rewritten to:

$$h_j = k(c/2)^{-1} \tag{48}$$

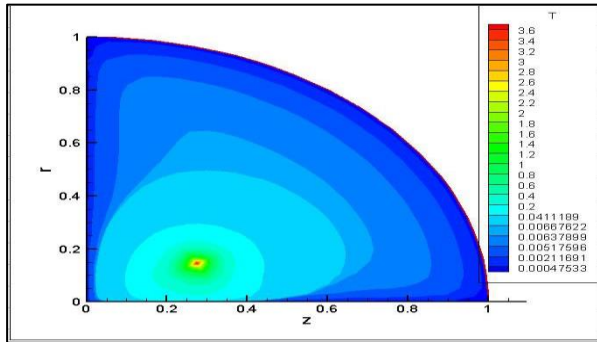
The required G_p was determined to be similar to that of the previous examination, and the results of this examination are shown in Fig. 10.

With the aim of calculating the function of G_p , the conjugate gradient method is applied and the results is shown in Fig. 10. a., b. for both data without and with noise respectively. To endorse the achieved results, G_p is considered as the direct input of the problem and same as previous examination the temperature distribution at selected point is found.

Fig. 11 shows the comparison of the estimated dimensionless temperature distribution with the exact

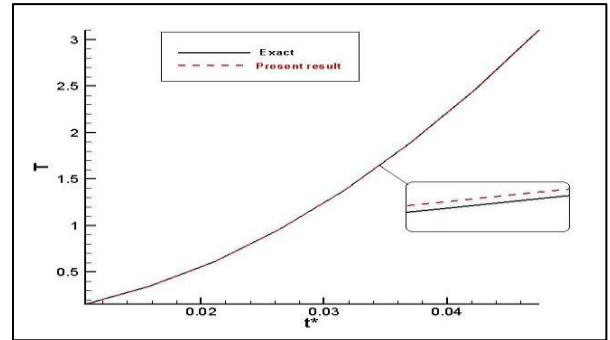


(a)

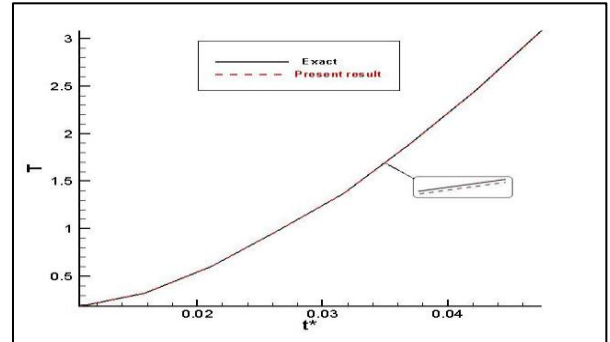


(b)

Figure 9. The related contours of the temperature distribution without noise (a) and with noise (b).

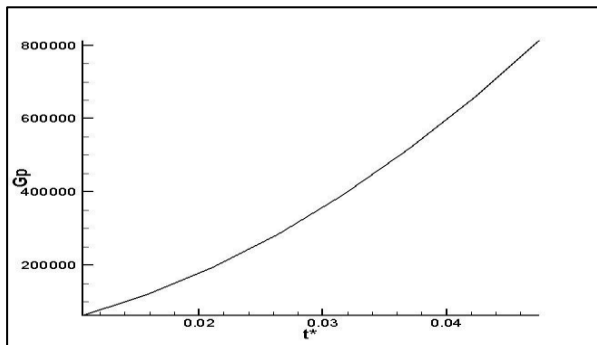


(a)

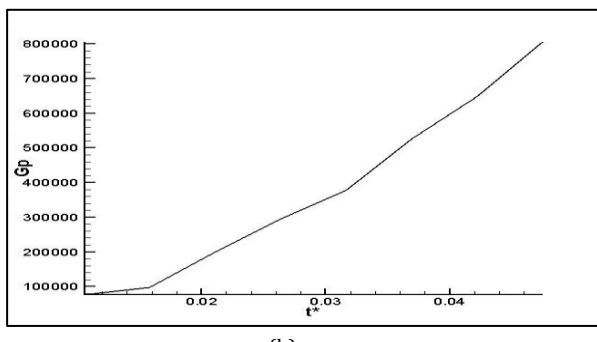


(b)

Figure 11. Comparison of the estimated dimensionless temperature distribution with the exact temperature distribution for both data without (a) and with noise (b) for a temperature distribution time of ~30 mins.

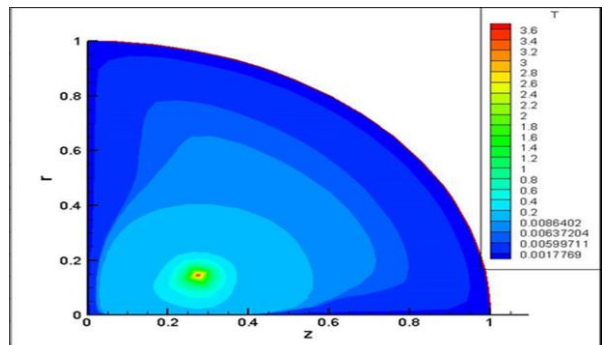


(a)

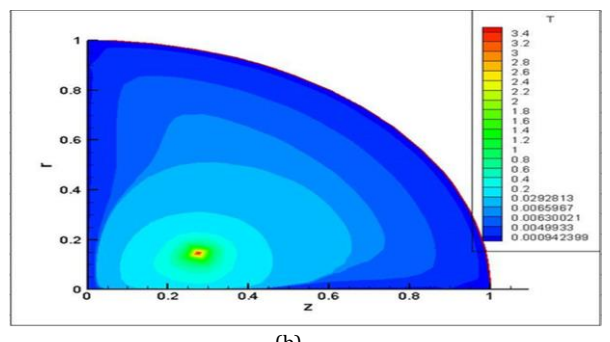


(b)

Figure 10. The estimated heating power source for data without noise (a) and with noise (b)



(a)



(b)

Figure 12. The related contours of the temperature distribution without noise (a) and with noise (b).

temperature distribution for both data with and without noise, while Fig. 12 shows the related temperature contours.

Similar to the previous examination, the results confirmed the high accuracy of the proposed method. It means the proposed method is time independent and the results bring acceptable accuracy in any heating time consideration. However, contours of temperature distribution in 30 minutes examination is more accurate compare to 10 minute examination. Perhaps, it is related to slower changes in temperature which makes it more accurate.

Conclusion

In this work, the adjoint problem in conjunction with the conjugate gradient method was used to solve the inverse heat conduction equation for predicting heating power sources. Two sensors measured the temperature distribution at two different points to increase the accuracy of the solution. The breast was represented by an axisymmetric model within the general coordinate system. The heat conduction in the breast tissue was modeled using the Pennes bioheat equation. Three different functions were employed to simulate the heating power source, and the results were highly accurate, and in order to further confirm this accuracy, the sharp corner and discontinuous functions, which are known to be very ill-posed, were used. The final results from the use of the previously mentioned functions confirmed that the proposed method is highly accurate in its prediction, with a noise in the input data of up to 1% present. The results confirm the efficiency of the proposed technique for predicting the time-dependent unidentified heating power source(s).

Nomenclature

- A; B; C tissue names in computational plane
- c constant
- C tissue specific heat (J Kg⁻¹ K⁻¹)
- P Pressure [bar]
- C_b the blood specific heat (J Kg⁻¹ K⁻¹)
- K tissue thermal conductivity (W·m⁻¹K⁻¹)
- ρ tissue density (Kg m⁻³)
- ρ_b blood density (Kg m⁻³)
- W_b the blood perfusion rate (Kg m⁻³ s⁻¹)
- T temperature (K)
- T_{a0} the arterial temperature (K)
- T_∞ ambient temperature to which living tissue has been exposed (K)
- q'''_m the metabolic heat generation rate (W·m⁻³)
- G_p(t) time-dependent heating power of source
- r normal distance from the z axis (m)
- z symmetric axis (m)
- δ Dirac deltafunction

- t time (s)
- R radial distance from center (m)
- α; β; γ computational coefficients
- n normal vector to the surface
- h heat transfer coefficient (W·m⁻² K⁻¹)
- d^k(t) direction of descent
- I number of measurements
- i; j node positions in computational plane
- J Jacobian transformation
- S objective function
- β^k search step size
- γ^k conjugate coefficient
- η vertical axis in computational plane
- λ adjoint temperature (K)
- ξ horizontal axis in computational plane
- σ standard deviation of measurement error
- ω standard deviation of normal distribution
- θ_∞ dimensionless constant temperature
- θ elevation temprature defined as $\frac{T-T_{a0}}{qR/K}$ (K)

Appendix

The transformation of the physical domain to the computational domain, as illustrated in Fig. 2.b, via the general coordinate technique [18] is as follow:

$$\theta_{z^*} = \frac{1}{J} (r_{\eta}^* \theta_{\xi} - r_{\xi}^* \theta_{\eta}) \tag{A1}$$

$$\theta_{r^*} = \frac{1}{J} (-z_{\eta}^* \theta_{\xi} - z_{\xi}^* \theta_{\eta}) \tag{A2}$$

$$\nabla^2 \theta = \frac{1}{J^2} [\alpha \theta_{\xi\xi} - 2\beta \theta_{\xi\eta} + \gamma \theta_{\eta\eta}] + [(\nabla^2 \xi) \theta_{\xi} + (\nabla^2 \eta) \theta_{\eta}] \tag{A3}$$

$$\alpha = z_{\eta}^{*2} + r_{\eta}^{*2} \tag{A4}$$

$$\beta = z_{\xi}^* z_{\eta}^* + r_{\xi}^* r_{\eta}^* \tag{A5}$$

$$\gamma = z_{\xi}^{*2} + r_{\xi}^{*2} \tag{A6}$$

$$\nabla^2 \xi = \frac{k_1 (r_{\xi\xi}^* z_{\eta}^* - z_{\xi\xi}^* r_{\eta}^*) + k_2 (r_{\xi\eta}^* z_{\eta}^* - z_{\xi\eta}^* r_{\eta}^*) + k_3 (r_{\eta\eta}^* z_{\eta}^* - z_{\eta\eta}^* r_{\eta}^*)}{J} \tag{A7}$$

$$\nabla^2 \eta = \frac{k_1 (z_{\xi\xi}^* r_{\eta}^* - r_{\xi\xi}^* z_{\eta}^*) + k_2 (z_{\xi\eta}^* r_{\xi}^* - r_{\xi\eta}^* z_{\xi}^*) + k_3 (z_{\eta\eta}^* r_{\xi}^* - r_{\eta\eta}^* z_{\xi}^*)}{J} \tag{A8}$$

$$k_1 = \frac{1}{J^2} (z_{\eta}^{*2} + r_{\eta}^{*2}) \tag{A9}$$

$$k_2 = \frac{-2}{J^2} (z_{\xi}^* z_{\eta}^* + r_{\xi}^* r_{\eta}^*) \tag{A10}$$

$$k_3 = \frac{1}{J^2} (z_{\xi}^{*2} + r_{\xi}^{*2}) \tag{A11}$$

$$\xi_{z^*} = \frac{1}{J} r_{\eta}^* \tag{A12}$$

$$\xi_{r^*} = -\frac{1}{J} z_{\eta}^* \tag{A13}$$

$$\eta_{z^*} = -\frac{1}{J} r_{\xi}^* \tag{A14}$$

$$\eta_{r^*} = \frac{1}{J} z_{\xi}^* \quad (A15)$$

$$J = z_{\xi}^* r_{\eta}^* + r_{\xi}^* z^* \quad (A16)$$

References

- [1] A. O. M., Inverse problems in identification and modeling of thermal processes: Russian contributions. *International Journal of Numerical Methods for Heat & Fluid Flow* 27, 711-728 (2017).
- [2] J. Dutta, B. Kundu, A revised approach for an exact analytical solution for thermal response in biological tissues significant in therapeutic treatments. *Journal of Thermal Biology* 66, 33-48 (2017).
- [3] J. Dutta, B. Kundu, Two-dimensional closed-form model for temperature in living tissues for hyperthermia treatments. *Journal of Thermal Biology* 71, 41-51 (2018).
- [4] O. M. Alifanov, *Inverse heat transfer problems*. (Springer Science & Business Media, 2012).
- [5] H. H. Pennes, Analysis of tissue and arterial blood temperatures in the resting human forearm. *Journal of applied physiology* 1, 93-122 (1948).
- [6] P. Vernotte, Les paradoxes de la theorie continue de l'equation de la chaleur. *compte Rendus* 246, 3154-3155 (1958).
- [7] C. Cattaneo, A form of heat conduction equation which eliminates the paradox of instantaneous propagation. *Comptes Rendus* 247, 431-433 (1958).
- [8] D. Y. Tzou, A Unified Field Approach for Heat Conduction From Macro- to Micro-Scales. *Journal of Heat Transfer* 117, 8-16 (1995).
- [9] W.-Q. Lu, J. Liu, Y. Zeng, Simulation of the thermal wave propagation in biological tissues by the dual reciprocity boundary element method. *Engineering Analysis with Boundary Elements* 22, 167-174 (1998).
- [10] A. Zolfaghari, M. Maerefat, A new simplified thermoregulatory bioheat model for evaluating thermal response of the human body to transient environments. *Building and Environment* 45, 2068-2076 (2010).
- [11] H. Ahmadikia, R. Fazlali, A. Moradi, Analytical solution of the parabolic and hyperbolic heat transfer equations with constant and transient heat flux conditions on skin tissue. *International communications in heat and mass transfer* 39, 121-130 (2012).
- [12] T.-C. Shih, P. Yuan, W.-L. Lin, H.-S. Kou, Analytical analysis of the Pennes bioheat transfer equation with sinusoidal heat flux condition on skin surface. *Medical Engineering & Physics* 29, 946-953 (2007).
- [13] P. Yuan, H.-E. Liu, C.-W. Chen, H.-S. Kou, Temperature response in biological tissue by alternating heating and cooling modalities with sinusoidal temperature oscillation on the skin. *International Communications in Heat and Mass Transfer* 35, 1091-1096 (2008).
- [14] M. M. Tung, M. Trujillo, J. A. López Molina, M. J. Rivera, E. J. Berjano, Modeling the heating of biological tissue based on the hyperbolic heat transfer equation. *Mathematical and Computer Modelling* 50, 665-672 (2009).
- [15] R. M. Cotta, B. P. Cotta, C. P. Naveira-Cotta, G. Cotta-Pereira, Hybrid integral transforms analysis of the bioheat equation with variable properties. *International Journal of Thermal Sciences* 49, 1510-1516 (2010).
- [16] H.-L. Lee, T.-H. Lai, W.-L. Chen, Y.-C. Yang, An inverse hyperbolic heat conduction problem in estimating surface heat flux of a living skin tissue. *Applied Mathematical Modelling* 37, 2630-2643 (2013).
- [17] M. Mohammadiun, Time-Dependent Heat Flux Estimation in Multi-Layer Systems by Inverse Method. *Journal of Thermophysics and Heat Transfer* 30, 599-607 (2016).
- [18] M. Mohammadiun, A. B. Rahimi, Estimation of time-dependent heat flux using temperature distribution at a point in a two layer system. *Scientia Iranica* 18, 966-973 (2011).
- [19] M. Mohammadiun, A. B. Rahimi, I. Khazaee, Estimation of the time-dependent heat flux using the temperature distribution at a point by conjugate gradient method. *International Journal of Thermal Sciences* 50, 2443-2450 (2011).
- [20] A. Jalali, Ayani, M. B., Baghban, M., Simultaneous estimation of controllable parameters in a living tissue during thermal therapy. *Journal of thermal biology* 45, 37-42 (2014).
- [21] L. A. Kengne, E. Bioheat transfer problem for one-dimensional spherical biological tissues. *Mathematical Bioscience* 269, 1-9 (2015).
- [22] M. B. A. M. Baghban, Source term prediction in a multilayer tissue during hyperthermia. *ELSEVIER, Journal of Thermal Biology* 52, 187-191 (2015).
- [23] E. Y. Ng, and Sudharsan, N. M., An Improved Three-Dimensional Direct Numerical Modelling and Thermal Analysis of a Female Breast with Tumour. *Journal of Engineering in Medicine*, 215, 25-37 (2001).
- [24] A. Amri, Saidane, A., and Pulko, S., Thermal Analysis of a Three-Dimensional Breast Model with Embedded Tumour using the Transmission Line Matrix (TLM) Method.

- Computers in Biology and Medicine 41, 76-86 (2011).
- [25] N. M. Sudharsan, and Ng, E. Y., Parametric Optimization for Tumour Identification: Bioheat Equation using ANOVA and the Taguchi Method., *Journal of Engineering in Medicine* 5, 505-512 (2000).
- [26] M. P. Cetingul, and Herman, C., A Heat Transfer Model of Skin Tissue for the Detection of Lesions: Sensitivity Analysis. *Physics in Medicine and Biology*, 55, 5933-5951 (2010).
- [27] L. Jiang, Zhan, W., and Loew, M. H., Modeling Static and Dynamic Thermography of the Human Breast Under Elastic Deformation. *Physics in Medicine and Biology* 56, 187-202 (2011).
- [28] O. R. B. Ozisik M.N., *Inverse Heat Transfer*. Taylor & Francis, NewYork., (2000).
- [29] Ozisik M.N., *Heat Conduction*. second ed. Wiley, New York., (1993).
- [30] J. Daniel, *The approximate minimisation of functionals* Prentice-Hall. Inc., Englewood Cliffs, NJ, (1971).
- [31] O. M. Alifano, *Inverse Heat Transfer Problems*. Springer-Verlag, New York., (1994).
- [32] N. T. H. Jiang B.H., Prud'homme M., Control of the boundary heat flux during the heating process of a solid material. *Int.Commun. Heat. Mass.* 32, 728-738 (2005).